J Mater Sci (2012) 47:521–529
DOI 10.1007/s10853-011-5829-5

Kinetics of orthorhombic martensite decomposition in TC21 alloy under isothermal conditions

Bin Tang · Hong-Chao Kou · Yi-Hong Wang · Zhi-Shou Zhu · Feng-Shou Zhang · Jin-Shan Li

Received: 6 May 2011 / Accepted: 27 July 2011 / Published online: 6 August 2011

Abstract The kinetics of martensite decomposition in TC21 alloy was investigated at isothermal conditions in the temperature range 500–850 °C. The dilatometry technique was utilized to trace the transformation process for different aging temperatures. Within the framework of the Avrami theory, the analysis of the experimental data was made by means of the Johnson–Mehl–Avrami (JMA) equation. A very good correspondence between the calculated and the experimental results was found. The JMA kinetic parameters obtained from different aging temperatures implied different mechanisms of the transformation. The α'' phase transforms to $\alpha + \alpha''$ (rich) at 500 °C and the transformation is incomplete. Further increase of the temperature to 800 and 850 °C results in directly transformation $\alpha'' \rightarrow \alpha + \beta$. The mechanism of the transformation alters during the course of the transformation for 550, 600, 650, 700, and 750 °C. Moreover, The TTT diagram was constructed for the martensite decomposition in TC21 alloy based on the dilatometry analysis and JMA theory, respectively. Good agreement between experimental and calculated TTT diagram is observed.

B. Tang (✉) · H.-C. Kou · Y.-H. Wang · J.-S. Li
State Key Laboratory of Solidification Processing, Northwestern Polytechnical University, Xi'an 710012, China
e-mail: toby198489@163.com

Z.-S. Zhu
Beijing Institute of Aeronautical Materials, Beijing 100095, China

F.-S. Zhang
Western Superconducting Technologies Co. Ltd., Xi'an 710021, China

Introduction

TC21 (Ti–6Al–2Sn–2Zr–3Mo–1Cr–2Nb–*x*Si, wt%) titanium alloy is a new ($\alpha + \beta$) titanium alloy with high strength, toughness, and damage-tolerance properties, which develops for structural application in advanced aircraft and aerospace [1]. Recently, lots of the researches have concentrated on determining the best methods of processing this alloy to produce an optimum combination of mechanical properties [2–4]. However, the mechanical properties improved by the thermo-mechanical and thermohydrogen treatments are controlled by the phase transformation and microstructure evolution.

The phase transformation and microstructure of TC21 alloy are sensitive to aging temperature and heating history [5]. In this alloy, quenching from a wide range of solution temperature (840–1000 °C) has been found to result in the formation of orthorhombic α'' martensite in our former work [5]. The α'' martensite is a type of metastable phase similar with hexagonal α' martensite and ω phase [6, 7], which has been reported to occur in the quenching process for a wide variety of binary, ternary, and commercial titanium alloys [8–10]. Due to the sensitive influence on elastic modulus and mechanical properties [11], the formation of α'' martensite in quenching and deforming process, and the decomposition during aging treatments have been investigated in binary and some commercial titanium alloys [12–14]. Besides, for such ($\alpha + \beta$) titanium alloys, the impurity concentrations (O) and major alloying elements have important influence on martensitic transformation [15]. Therefore, the concentrations of major elements and impurities of the samples were limited in an appropriate range in this work.

In order to reveal the relationship between the microstructure and mechanical properties of TC21 alloy, it is

necessary to investigate the heat treatment conditions and decomposition behavior of α'' martensite.

In this study, the metallurgical aspects of the phase constitutions of quenched (from β phase) structures, the reverse transformation kinetics of the martensite α'' to α and β phases with isothermal aging treatment, and the TTT diagram for martensite decomposition are investigated by optical microscopy (OM), X-ray diffraction (XRD), transmission electron microscopy (TEM), and dilatometry tests with regard to TC21 alloys. Furthermore, in order to predict the phase transformation kinetics with details, the theoretical frame of Johnson–Mehl–Avrami (JMA) theory is utilized, and the JMA kinetics parameters and local activation energy are obtained. These parameters can be used in the heat treatment practice of the TC21 alloy to predict and trace the course of martensite decomposition at different aging conditions.

Experimental procedures

The TC21 alloy used in the experiment was obtained in the form of bars with 210 mm in diameter from Western Superconducting Technologies Co., Ltd., China. The bars were supplied in a hot forging condition with beta transus temperature of 960 °C, given a α/β solution heat treatment at 900 °C for 2 h, cooled in air and then annealed at 590 °C for 4 h.

The samples cut from the forged bars were solution treated at 1000 °C for 30 min and followed by water quenching. The quenching microstructure and phase constitution of the TC21 specimens were detected by OM (DM-2500M), XRD, and TEM techniques. Room temperature XRD was carried out in the equipment of PANalytical X'Pert PRO with Cu Kα radiation at 40 kV and 30 mA, the scanning rate being 0.002° per step from $2\theta = 25°$–$75°$. For TEM study, the 3 mm diameter rods of TC21 alloy were electro-polished using a twin jet electro-polisher in solution bath consisting of 200 mL methanol, 100 mL butanol, and 15 mL perchloric acid under the voltage and temperature conditions of 30–40 V and −40 °C. The TEM foils were studied in H-800 electron microscope with an operating voltage of 175 kV. The dilatometry tests were carried out in Gleeble 3500. The samples were heated up to corresponding isothermal temperatures quickly and hold on for a designed time in the range of 200–9300s, followed by quenching to water. The aging temperatures were set to 500, 550, 600, 650, 700, 750, 800, and 850 °C, respectively. In order to avoid the effect of the phase transformation during the heating process, the heating rate was set to 100 °C/s.

Results and discussion

The Microstructure after quenching

The chemical composition of the received TC21 alloy is shown in Table 1. Note that the impurity concentrations of the prepared samples were in the proper range. The microstructure and phase constitution of the sample after quenching from 1000 °C are illustrated in Fig. 1. As can be seen the quenched structure consists of a mixture of orthorhombic α" martensite plus small amount of α_2 phase (Ti_3Al) and residual body-centered-cubic (bcc) β phase. Fine needle-like traces of α'' martensite are observed in the prior β grain, as shown in Fig. 1a. However, the details of the α'' martensite investigated by TEM (Fig. 1b) show that the α'' martensite is constituted by platelets with the stacking faults inside it. Figure 1c shows the selected area diffraction pattern (SADP) of $[\bar{1}\bar{4}3]\alpha''$ zone, which confirms the presence of α_2 phase. The weak peaks of α_2 and residual β phases in the diffraction pattern predict that the amount of this two phases is so small in the mixture structures that the quenched structure of TC21 alloy is dominated by α'' martensite. The lattice parameters of the α'', α_2, and β phases after quenching from 1000 °C for TC21 alloy are list in Table 2.

Dilatometry tests

The phase transformation introduced volume changes of polycrystalline titanium alloys can be generally considered to be isotropic [16]. Thus, the lever rule can be used to handle the heating expansion curve to explore the relation between the transformed volume fraction and the time for different aging temperatures.

In order to analyze the α'' martensite decomposition reaction in the TC21 alloy in details, eight aging temperatures in a large range below the β transus temperature, were selected from the dilatometric curve during continuous heating process [17], in the range from 500 to 850 °C.

The variation of diameter, Δd, can be calculated by

$$\Delta d = \Delta d_0 - \Delta d_t \quad (1)$$

Table 1 Chemical composition of received TC21 alloy (wt%)

Elements	Al	Sn	Zr	Mo	Cr	Nb	Si	C	H	O	N	Fe
Content	5.8	2.0	1.8	2.7	1.2	2.2	0.14	0.05	0.007	0.12	0.04	0.08

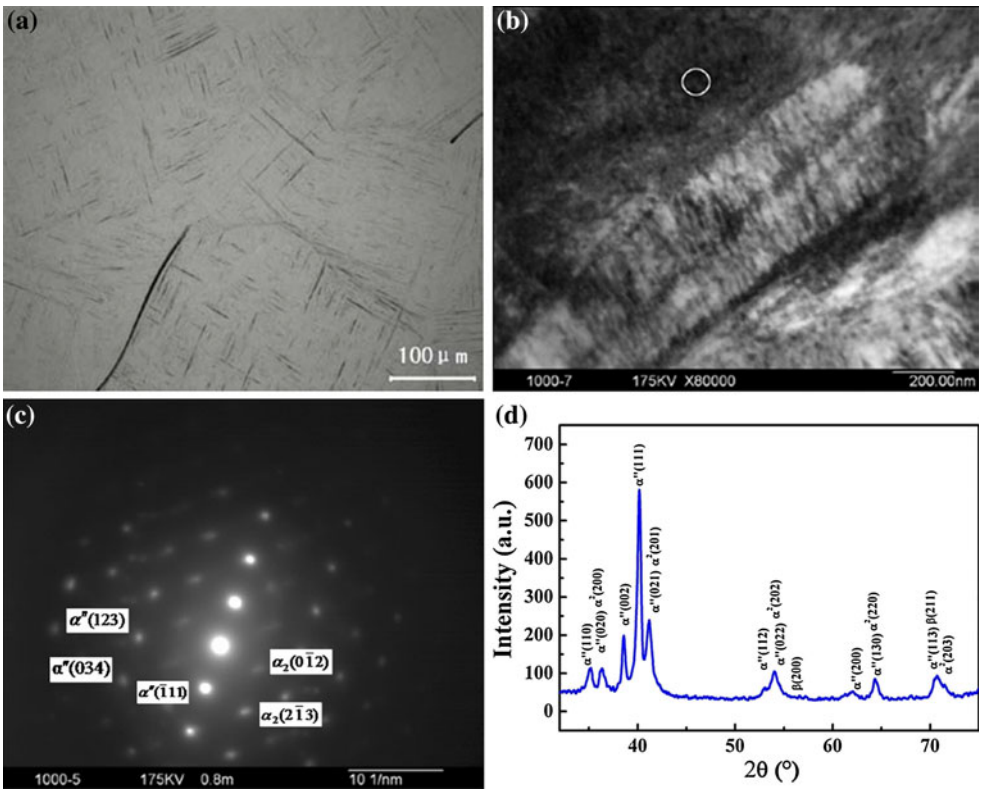

Fig. 1 Microstructure and phase constitution of TC21 alloy after solution treated at 1000 °C for 30 min and water quenching. **a** Optical micrographs, **b** TEM micrographs, **c** SADP taken from the (**b**). **d** X-ray diffraction patterns

Table 2 Lattice constants of α'', α_2, and β phase for TC21

Phase	a (nm)	b (nm)	c (nm)
α''	0.2978	0.4984	0.4689
α_2	0.5689		0.4655
β	0.3270		

Where Δd_0 is the initial variation of diameter before aging and Δd_t is the variation of diameter from initial state to time t.

Figure 2 shows the variations of diameter of specimens versus aging time curves obtained for the alloy aged at 500, 550, 600, 650, 700, 750, 800 and 850 °C. As shown in Fig. 2, the diameters decrease with time at first and then tend to balance at last. Note that the same process is found for all curves in the considered temperature range. Moreover, there is an inversely proportional relationship between the decomposition period and the aging temperature. When the samples are aging at 500 °C, the rate of the transformation is very slow and it needs 9 ks to finish. Further increase of the temperature to 850 °C results in decrease of the transformation time (estimated to be around 180 s). In addition, the variations of diameter are larger for higher aging temperature, indicates that the amount of total transformation is larger at high temperature.

Kinetics of decomposition of the orthorhombic martensite

According to the results of dilatometry test, the transformed volume fraction, f, is assumed to be given by the ratio of the observed dilatation to the maximum possible dilatation at transformation time of t:

$$f = \frac{\Delta d}{\Delta d_0 - \Delta d_{\max}} \tag{2}$$

where f is the product volume fraction which varies with time t, and $\Delta d_{\max}$ is the total variation of diameter during the phase transformation process.

The results from the dilatometry study (Fig. 2) trace the kinetics of martensite decomposition in TC21 alloy at the temperatures studied. According to Eq. 2, the experimental dilatometric curves were recalculated to give the fraction of transformation versus time (see Fig. 3).

In this study, the kinetics of the martensite decomposition in TC21 alloy was modeled by adapting the classic JMA theory [18–21], and the kinetic parameters of phase transformation were subsequently calculated.

The decomposition process of martensite at special temperatures in TC21 alloy is controlled by diffusion. For this particular case, a popular JMA equation was used.

$$f = 1 - \exp(-Kt^n) \tag{3}$$

With

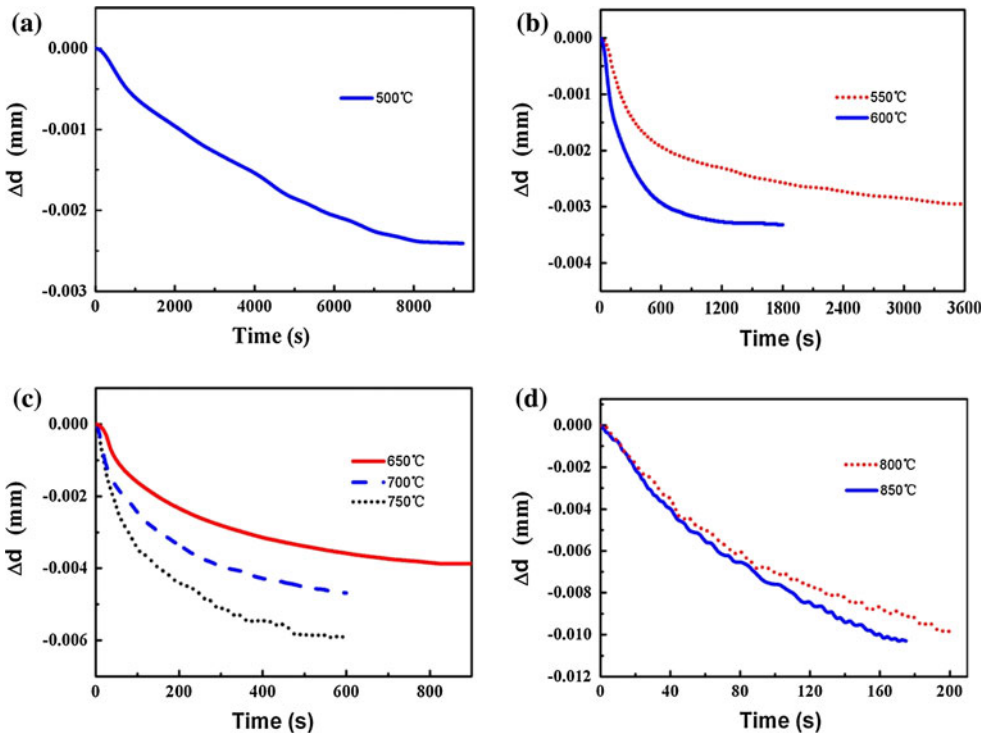

Fig. 2 Diameter changes versus aging time for the TC21 alloy isothermal exposure at **a** 500 °C, **b** 550–600 °C, **c** 650–750 °C, and **d** 800–850 °C

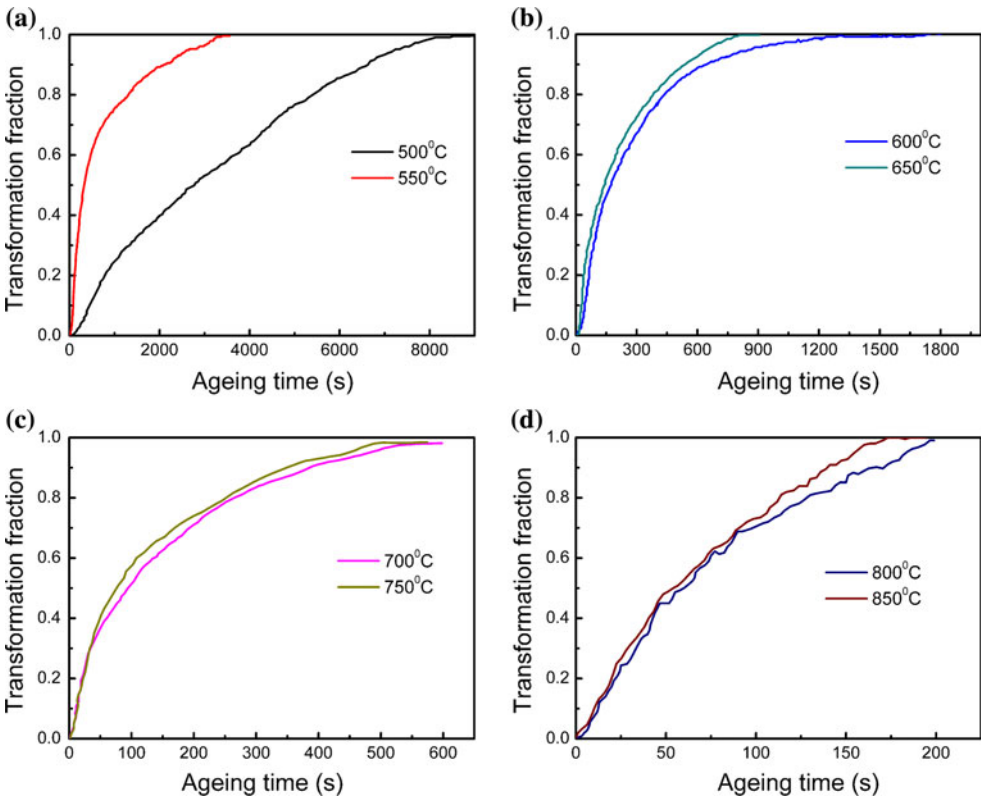

Fig. 3 Kinetics of the martensite decomposition at different temperatures of isothermal exposure for TC21 alloy

$$f = \frac{f(t)}{f(\max)} \tag{4}$$

$$K = k_0 \exp\left(-\frac{E}{RT}\right) \tag{5}$$

where K is the reaction rate constant and n is the Avrami exponent that describes the nucleation and growth mechanisms. $f(t)$is the amount of martensite decomposition after a time t. $f(\max)$ is the maximum volume fraction of the

decomposition at the corresponding temperature of the transformation. E is local activation energy.

Equations 3 and 4 were used to analyze the experimental data by means of logarithmic plots,

$$\ln\left(\ln\left(\frac{1}{1-f}\right)\right) = \ln(K) + n\ln(t) \quad (6)$$

Based on Eq. 6, the n and K values for all studied temperatures could be derived for TC21 alloy. The plots $\ln\left(\ln\left(\frac{1}{1-f}\right)\right)$ against $\ln(t)$ are presented in Fig. 4 for 500 °C (Fig. 4a), 550–750 °C (Fig. 4b), and 800–850 °C (Fig. 4c). In such plots, the slope of the resulting straight line gives the Avrami exponent n and the intercept gives the value of K. The n and K values obtained from slope of straight line in Fig. 4 are presented in Table 3. Note that the noticeable distinction of Avrami exponent n exists between different aging temperatures. For lower temperature (500 °C) and highest studied temperatures (800 and 850 °C), there is nearly a linear relationship between the $\ln\left(\ln\left(\frac{1}{1-f}\right)\right)$ and $\ln(t)$ (see Fig. 4a, c), and n is determined as a constant in the range of 1.12–1.19. This indicates that the saturation of nucleation and diffusion-controlled three-dimensional grain growth are responsible for the martensite decomposition [22]. Besides, it also suggests that the mechanism of the transformation does not change in the course of the transformation for 500, 800, and 850 °C.

Figure 5 shows the microstructure and phase constitution of TC21 alloy after isothermal treated at 500 °C. Note that the α'' phase transforms to $\alpha + \alpha''$ (rich) phases after the dilatometry test and the phase transformation aged at this temperature is incomplete. The TEM observations (Fig. 5b, c) show that the α phase homogenous precipitates inside the stacking faults of α'' phase. Additional aging for 4 h at the same temperature was applied to the sample after dilatometry experiments. The XRD pattern shown in Fig. 5d suggests that the α'' (rich) continue transform to $\alpha + \beta$ phase after this additional aging.

Although the shape of plot $\ln\left(\ln\left(\frac{1}{1-f}\right)\right)$ versus $\ln(t)$ at 800 and 850 °C (Fig. 4c) is similar to the result for aging at 500 °C, the mechanisms of the transformation are different. Figure 6 illustrates the XRD patterns of TC21 alloy after isothermal treated at 800 and 850 °C. Note that α'' phase directly transform to $(\alpha + \beta)$ phases for isothermal exposure at 800 and 850 °C.

However, when the aging temperature is in the range of 550–750 °C, the $\ln\left(\ln\left(\frac{1}{1-f}\right)\right)$ versus $\ln(t)$ plot consists of two straight lines with an intermediate region over which the slope decrease. In the early stage, the Avrami exponent n varies with the temperatures in the range of 1.5–2.06 corresponding to saturation nucleation and diffusion-controlled growth of precipitates. It also indicates that the grain boundaries play a minor role in the overall

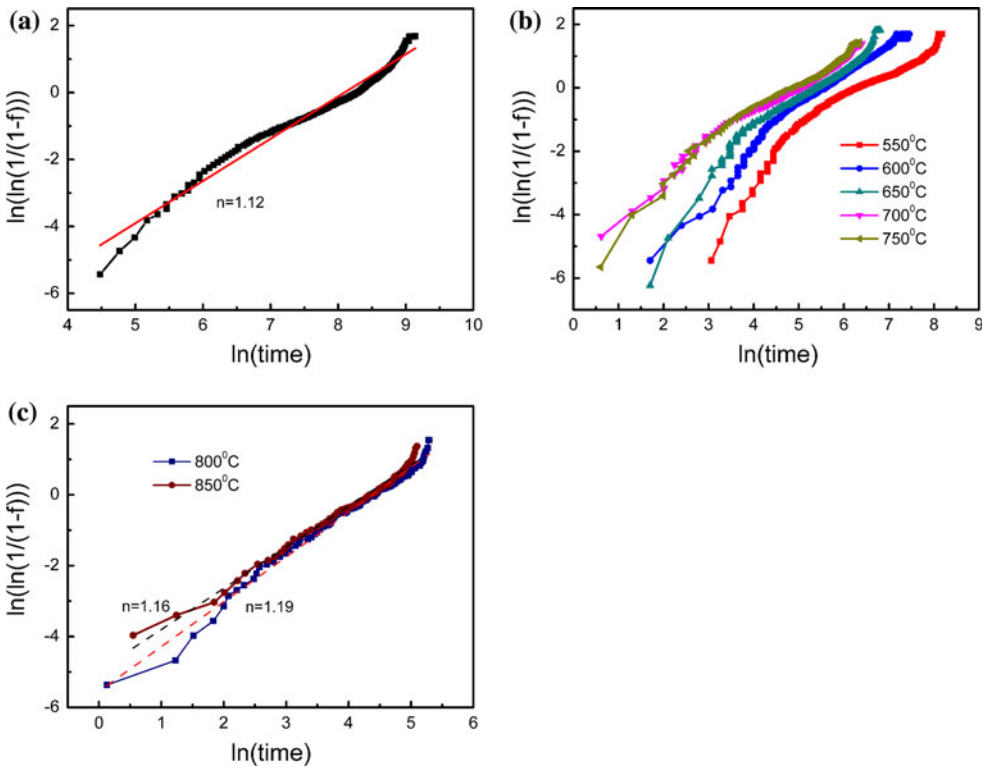

Fig. 4 Plots of $\ln\left(\ln\left(\frac{1}{1-f}\right)\right)$ versus $\ln(t)$ for deriving the JMA parameters for TC21 alloy at **a** 500 °C, **b** 550–750 °C, and **c** 800–850 °C

Table 3 Kinetic parameters and local activation energies results for the α'' martensite decomposition of TC21 alloy from dilatometry measurements for the different isothermal conditions

T (°C)	Transformation process				
	Early stage			Large stage	
	n	K	E (kJ/mol)	n	K
500	1.12	1.15×10^{-4}	167.122	1.12	1.15×10^{-4}
550	1.93	1.59×10^{-5}		0.74	8.40×10^{-3}
600	1.94	6.57×10^{-5}		0.89	6.87×10^{-3}
650	2.06	1.01×10^{-4}		0.84	1.11×10^{-2}
700	1.76	1.19×10^{-3}		0.8	2.02×10^{-2}
750	1.5	2.61×10^{-3}		0.77	2.33×10^{-2}
800	1.16	6.15×10^{-3}		1.16	6.15×10^{-3}
850	1.19	5.98×10^{-3}		1.19	5.98×10^{-3}

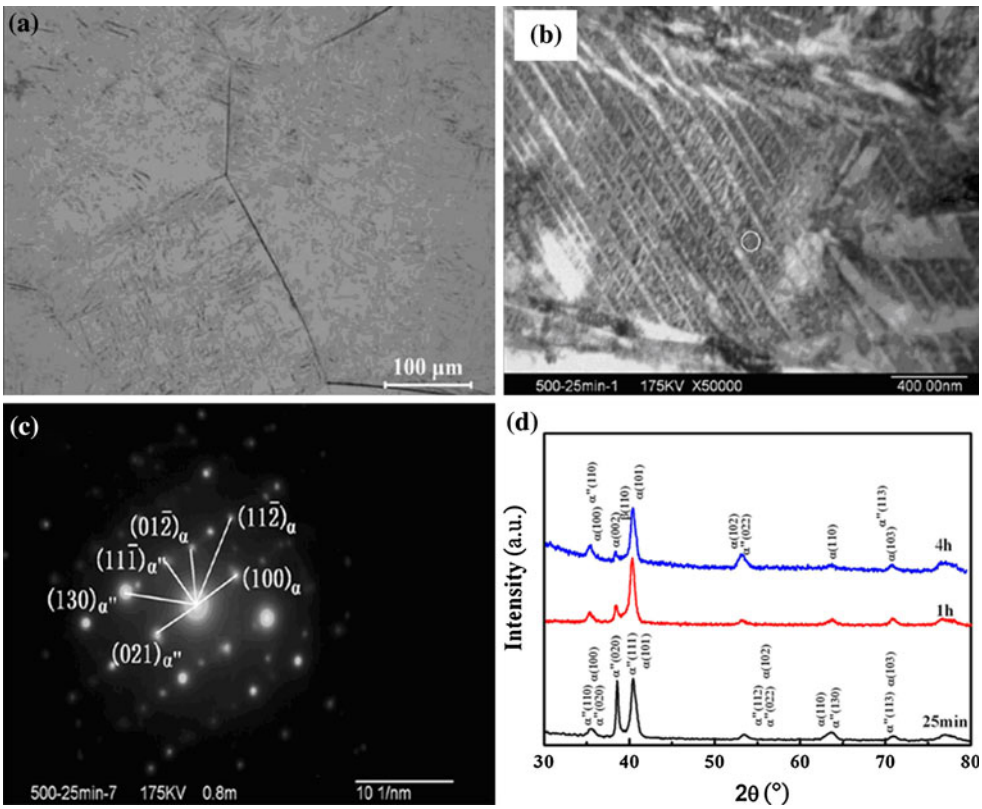

Fig. 5 Microstructure and phase constitution of TC21 alloy after isothermal treated at 500 °C. **a** Optical micrograph after aging for 1 h. **b** TEM micrograph and **c** diffraction pattern after isothermal treated 25 min. **d** XRD patterns after aging for 25 min, 1 h, and 4 h

precipitation process [23]. With the time increase, there was an obvious tendency for change of the line slope (see Fig. 4b; Table 3) to lower values about 0.74–0.89. Note that the mechanism of the transformation alters during the course of the transformation for 550, 600, 650, 700, and 750 °C. Similar result has been reported in Ti-1023, Ti-6246, and β21s alloys as well [24, 25].

According to above discussion, the decomposition mechanisms of martensites at low and high temperature are strikingly different. For lower temperature (500 °C) results from dilatometry test ($n = 1.12$) show that the α phase saturated nucleate at the defects (stacking faults) of α'' phase and the phase transformation $\alpha'' \rightarrow \alpha + \alpha''$ (rich) is in condition of slow diffusion-controlled growth of vary fine α phase. Increase the aging temperatures to 550–750 °C, n values have two stages corresponding to two transformation mechanisms. In the first stage, the n values change from 1.93 to 2.06 and subsequently to 1.5 with temperature increase. It indicates that the transformation mechanism of TC21 alloy in this temperature range sensitively depends

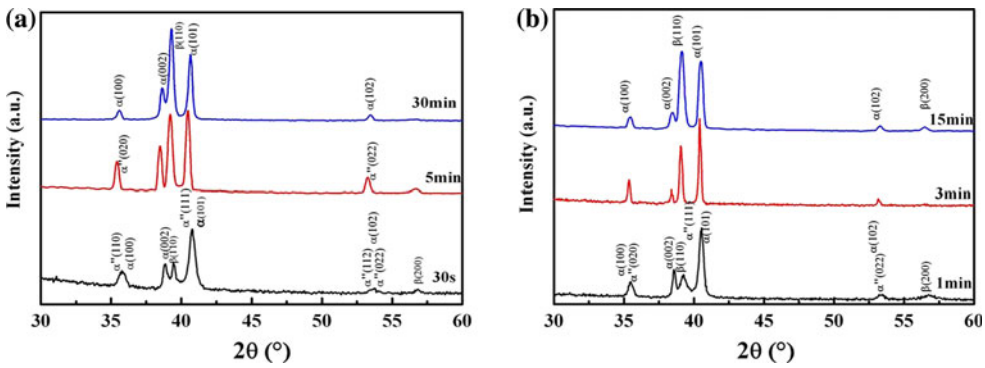

Fig. 6 The XRD patterns of TC21 alloy after isothermal treated at **a** 800 °C and **b** 850 °C for different times

on the temperature and changes gradual from one to another. Aging at these temperatures, different transformation sequences will happen, such as $\alpha'' \rightarrow \alpha + \alpha''$ (rich) $\rightarrow \alpha + \beta$ and $\alpha'' \rightarrow \alpha' + \beta$ (rich) $\rightarrow \alpha + \beta$. However, further increase the aging temperature to 800–850 °C, single transformation mechanism is obtained with values of about 1.16 and 1.19. Although they have similar values with the result from aging at 500 °C, the detail mechanisms of the transformation are different. The α and β phases co-nucleate from α'' matrix and the particles grow rapidly controlled by faster diffusion.

According to above calculation results, we take $\ln(K)$ as a function of $\frac{1}{T}$. The Eq. 5 can be rewritten as

$$\ln(K) = \ln(k_0) - \frac{E}{RT} \tag{7}$$

So, a linear relationship between $\ln(K)$ and $\frac{1}{T}$ is expected and the value of the activation energy for the transformation process can be obtained from the slope of this straight line. Figure 7 illustrates the plot of $\ln(K)$ versus $\frac{1}{T}$and from this one the local activation energy, E, of the α'' martensite decomposition is obtained $E = 167.122$ kJ/mol.

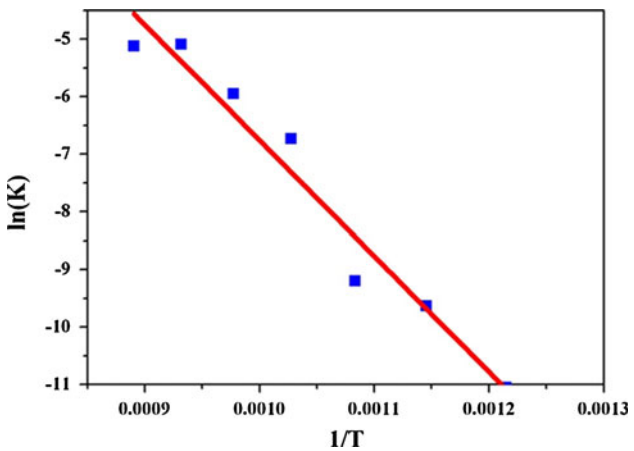

Fig. 7 Plot of $\ln(K)$–$1/T$ for the decomposition of martensite of TC21 alloy

The derived JMA parameters allow the transformation kinetics to be calculated for different temperatures. Based on the n and K values list in Table 3, the transformation fractions of α'' martensite decomposition at different aging temperatures were calculated and the corresponding curves were presented in Fig. 8.

As shown in Fig. 8, the transformation curves at eight isothermal temperatures seem to be identical with a slight distinction between calculation results and experimental measurements. The distinction within ±3% error range is appeared at the end of transformation when the temperature loads at 500, 750, 800, and 850 °C. In general, there is a good agreement between the calculated and the experimentally measured transformed fractions.

Time–temperature-transformation diagram

The Time–temperature-transformation (TTT) diagram gives the relationship between the temperature and the time for a fixed fractional amount of transformation to be attained. Such diagrams are usually used in alloy heat treatment practice. Using the dilatometry results on the kinetics of martensite decomposition at different aging temperatures the TTT diagrams are designed and presented in Fig. 9a. In this study, the transformation fractions of 5 and 95% for the start and the end of the transformation were used. It should be noted that the end of the transformation means the degree of decomposition. For examples, the final product is a mixture of α and α'' (rich) when isothermal treated at 500 °C. While the phase composition is $(\alpha + \beta)$ when aging at 850 °C. Figure 9b shows the calculated kinetics of the martensite decomposition in the theoretical frame of the JMA theory. Note that an acceptable correspondence between the experimental and calculated results is found.

Conclusions

The kinetics of α'' martensite decomposition in TC21 alloy was studied at isothermal conditions using dilatometry

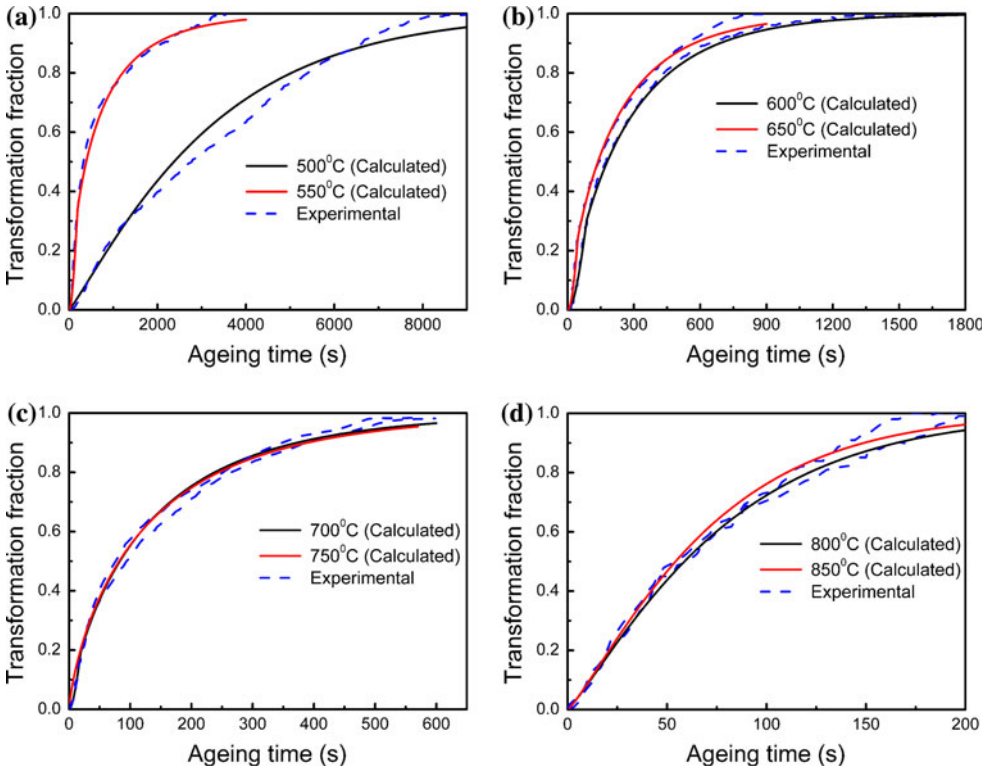

Fig. 8 Calculated and experimental kinetics of the martensite decomposition at different aging temperatures for TC21 alloy. **a** 500–550 °C, **b** 600–650 °C, **c** 700–750 °C, and **d** 800–850 °C

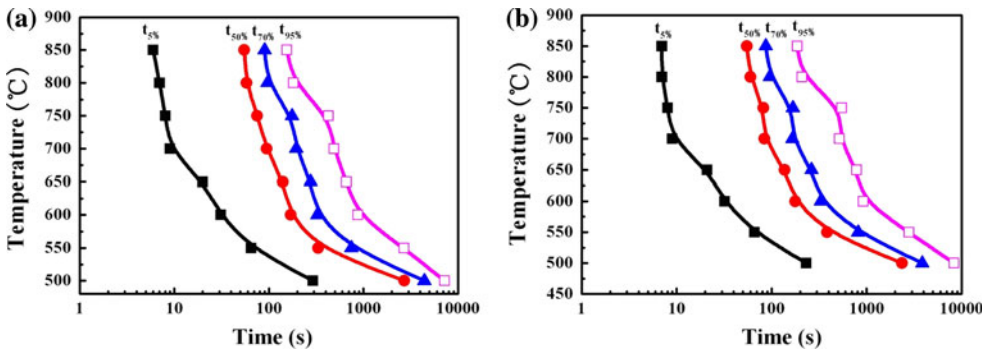

Fig. 9 Calculated (**a**) and experimental (**b**) TTT diagrams of the martensite decomposition for TC21 alloy

measurements. Furthermore, in the frame of JMA theory, the kinetics of decomposition was modeled and the kinetic parameters were obtained for different aging temperatures. The main conclusions are:

(a) The martensite structure after quenching from 1000 °C consisted of a mixture of α'', α_2, and residual β phase. After isothermal exposure at different temperatures from 500 to 850 °C, the amount of decomposition increased with the time and it is sensitive to aging temperature.

(b) Different aging temperatures result in different transformation mechanisms for TC21 alloy. Aging at 500 °C for 9 ks produces no β phase and the transformation is dominated by $\alpha'' \rightarrow \alpha + \alpha''$ (rich). Additional longer time aging at this temperature suggests that α'' (rich) continue transform to $(\alpha + \beta)$ phases. Two mechanisms of the transformation are included when the aging temperature is elevated to 550–750 °C. Note that decreased nucleation and diffusion-controlled growth are responsible for the martensite decomposition. Further increase of the temperature to 800 and 850 °C, the martensite α'' directly decomposes into the co-precipitations of the $(\alpha + \beta)$ phases.

(c) The local activation energy of α'' martensite decomposition obtained by the JMA theory is 167.122 kJ/mol.

(d) There is a good agreement between the calculated and the experimentally measured transformed fractions and TTT diagrams.

Acknowledgement This study is supported by the fund of the State Key Laboratory of Solidification Processing in NWPU (Grant: 37-TP-2009) and 111 Project (No. B08040).

References

1. Qu HL, Zhou YG, Zhou L, Zhao YQ, Zeng WD, Feng L, Yang YQ, Chen J, Yu HQ, Li H, Zhang YN, Guo HC (2005) Trans Nonferrous Met Soc China 15:1120
2. Wang X, Zhao Y, Wang Y, Hou H, Zeng W (2010) J Alloys Compd 490:562
3. Zhu Y, Zeng W, Sun Y, Feng F, Zhou Y (2011) Comp Mater Sci 50:1785
4. Zhu Y, Zeng W, Feng F, Sun Y, Han Y, Zhou Y (2010) Mater Sci Eng A 528:1757
5. Wang Y, Kou H, Chang H, Zhu Z, Zhang F, Li J, Zhou L (2009) Mater Sci Eng A 508:76
6. Nag S, Banerjee R, Fraser H (2009) J Mater Sci 44:808. doi:10.1007/s10853-008-3148-2
7. Nag S, Banerjee R, Stechschulte J, Fraser HL (2005) J Mater Sci Mater Med 16:679
8. Tang X, Ahmed T, Rack HJ (2000) J Mater Sci 35:1805. doi:10.1023/A:1004792922155
9. Grujicic M, Zhang Y (2000) J Mater Sci 35:4635. doi:10.1023/A:1004826301287
10. Wyatt Z, Ankem S (2010) J Mater Sci 45:5022. doi:10.1007/s10853-009-4178-0
11. Hao Y, Yang R, Niinomi M, Kuroda D, Zhou Y, Fukunaga K, Suzuki A (2002) Metall Mater Trans A 33:3137
12. Zhou YL, Niinomi M, Akahori T (2004) Mater Sci Eng A 384:92
13. Lee YT, Welsch G (1990) Mater Sci Eng A 128:77
14. Yang Y, Li GP, Cheng GM, Wang H, Zhang M, Xu F, Yang K (2008) Scr Mater 58:9
15. Zhang XD, Wiezorek JMK, Baeslack WA, Evans DJ, Fraser HL (1998) Acta Mater 46:4485
16. Szkliniarz W, Smolka G (1995) J Mater Process Technol 53:413
17. Wang Y, Kou H, Chang H, Zhu Z, Su X, Li J, Zhou L (2009) J Alloys Comp 472:252
18. Johnson WA, Mehl RF (1939) Trans Am Inst Miner Metall Eng 135:416
19. Avrami M (1939) J Chem Phys 7:1103
20. Avrami M (1940) J Chem Phys 8:212
21. Avrami M (1941) J Chem Phys 9:177
22. Christian JW (1975) The theory of transformations in metals and alloys. Pergamon Press, Oxford
23. Furlani AM, Stipcich M, Romero R (2005) Mater Sci Eng A 392:386
24. Bein S, Bechet J (1996) J Phys 6:99
25. Malinov S, Sha W, Markovsky P (2003) J Alloys Compd 348:110